Available online at www.sciencedirect.com
ScienceDirect
Journal of Nuclear Materials 367–370 (2007) 222–228
journal of nuclear materials
www.elsevier.com/locate/jnucmat

Pre- and post-deformation microstructures of oxide dispersion strengthened ferritic steels

R. Kasada [a,*], N. Toda [b], K. Yutani [b], H.S. Cho [b], H. Kishimoto [a], A. Kimura [a]

[a] *Institute of Advanced Energy, Kyoto University, Gokasho, Uji, Kyoto 611-0011, Japan*
[b] *Graduate School of Energy Science, Kyoto University, Gokasho, Uji, Kyoto 611-0011, Japan*

Abstract

Pre- and post-deformation microstructures and tensile properties of the newly-developed oxide dispersion strengthened (ODS) ferritic steels, K1 (Fe–19Cr–0.3W–0.3Ti–0.3Y_2O_3) and K4 (Fe–19Cr–4Al–2W–0.3Ti–0.3Y_2O_3) for nuclear fusion reactors and Generation IV nuclear fission systems were investigated. The nano-oxides of the K1 were cubic pyrochlore $Y_2Ti_2O_7$, while those of K4 were mainly perovskite $AlYO_3$, which was confirmed by transmission electron microscopy and X-ray diffraction (XRD) analyses. K1 was found to have much higher strength than K4 and the difference in the nano-oxides of K1 and K4 can account for this difference. Most of the extracted residues in the K1 and K4 identified by XRD consisted of $M_{23}C_6$ carbides.

1. Introduction

Since some commercial and experimental oxide dispersion strengthened (ODS) ferritic/martensitic (F/M) steels have shown excellent elevated-temperature strength and low void swelling [1,2], ODS F/M steels offer great promise for achieving higher operating temperatures than conventional F/M steels for use in fusion reactors and Generation IV nuclear fission systems. However, the previous ODS F/M steels were less appropriate for use as fuel cladding materials in corrosive coolant, such as super critical pressurized water (SCPW) and lead–bismuth eutectic. To achieve sufficient corrosion resistance in severe environments, we have been developing a new series of high Cr ODS ferritic steels [3–8]. It is found that the new ODS ferritic steels showed an excellent resistance against SCPW corrosion [5], hydrogen-induced embrittlement [6], liquid–metal corrosion [3] and stress corrosion cracking in hot-pressurized water [7]. Recent R&D efforts are presented in these proceedings.

The present paper focuses on the microstructure and tensile–deformation behavior of the newly developed high Cr ODS ferritic steels. ODS F/M steels have been produced with different alloy compositions and fabrication process, resulting in different microstructures, such as nano-oxide particles, precipitates, anisotropic grains and so on. This work analyses the microstructural features of the high Cr ODS ferritic steels. Effects of aluminum

* Corresponding author. Tel.: +81 774 38 3483; fax: +81 774 38 3479.
E-mail address: r-kasada@iae.kyoto-u.ac.jp (R. Kasada).

0022-3115/$ - see front matter © 2007 Elsevier B.V. All rights reserved.
doi:10.1016/j.jnucmat.2007.03.141

and titanium on the formation of nano-oxide particles and other precipitates in the ODS steels are discussed. Tensile–deformation behavior of the ODS ferritic steels was also investigated and correlated with microstructural analyses.

2. Experimental procedure

Two of the newly developed ODS ferritic steels produced by mechanical alloying methods were used in the present study. The chemical compositions are shown in Table 1. The nominal compositions of the K1 and K4 steels were Fe–19Cr–0.3W–0.3Ti–0.3Y_2O_3 and Fe–19Cr–4Al–2W–0.3Ti–0.3Y_2O_3, respectively. The obvious difference between the K1 and K4 is an addition of about 4 wt% aluminum, which can improve the corrosion resistance in liquid–metal environment, such as lead–bismuth eutectic [3]. The ODS ferritic steels were fabricated as cylindrical rods by hot-extrusion. After that, a homogenization heat treatment was performed at 1050 °C for 1 h followed by air cooling. Details of the fabrication process were given in [4].

Transmission electron microscope (TEM) observations were performed using a JEOL 2010, operating at 200 kV. Energy dispersion X-ray spectrometry (EDS) was carried out with a scanning TEM (STEM) mode. Specimens for TEM observation were prepared from sheet parallel to extruded direction, by electro-polishing using a twin-jet polishing machine. Foil thickness of the observed areas was determined by convergent beam diffraction. The structures of the extracted residues were determined by X-ray diffraction (XRD), using Cu Kα line.

Sheet type tensile specimens, with gauge dimensions 25 mm × 8 mm × 2.5 mm, were fabricated from the cylindrical rods. The tensile direction was parallel to longitudinal axis of the rod. Tensile tests were carried out at a strain rate of 6.67×10^{-5} s^{-1} at temperatures from room temperature to 800 °C in air. Post-deformation microstructures were also observed by TEM.

3. Results

3.1. Microstructure of the as-received ODS ferritic steels

TEM bright field (BF) images for the as-received K1 and K4 steels are shown in Fig. 1(a) and (b),

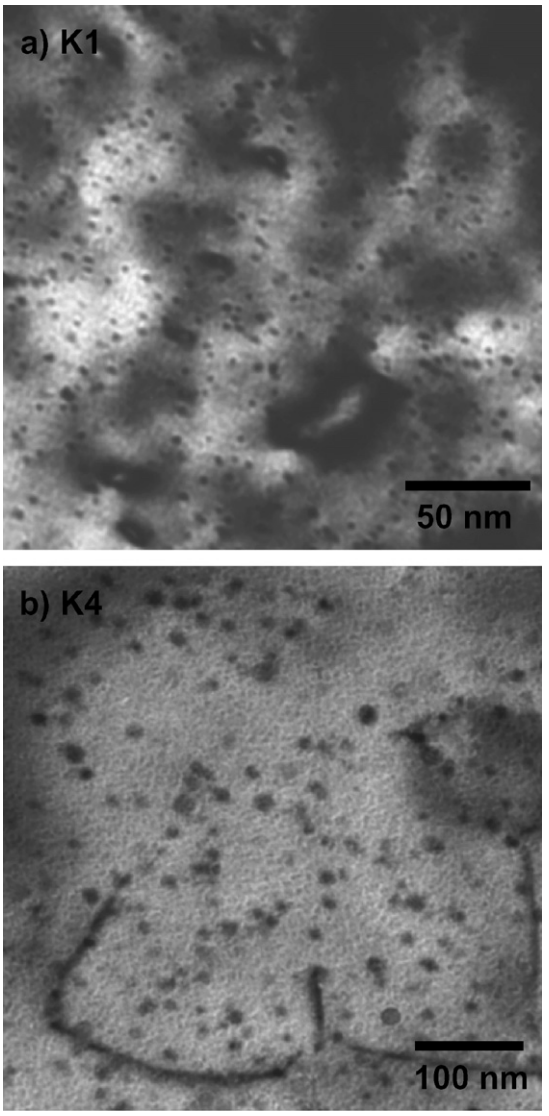

Fig. 1. TEM bright field images of as-received K1 and K4 steels.

Table 1
Chemical compositions of the ODS ferritic steels used in the present study (wt%)

Material	C	Si	Mn	P	S	Cr	W	Al	Ti	N	Y_2O_3
K1	0.05	0.041	0.06	<0.005	0.002	18.37	0.29	<0.01	0.28	0.014	0.368
K4	0.09	0.039	0.06	<0.005	0.002	18.85	1.83	4.61	0.28	0.005	0.368

respectively. The fine spherical particles in both images are considered to be nano-oxide particles. Size distributions of the nano-oxide particles in Fig. 2 were determined from a quantitative analysis of the TEM micrographs. The mean diameter and number density of the nano-oxide particles are 3.7 nm and 1.3×10^{23} m^{-3} for K1 steel, and 7.3 nm and 1.5×10^{22} m^{-3} for K4 steel, respectively. The chemical compositions of the particles as determined by STEM-EDS analyses are shown in Fig. 3. The particles in K1 contained yttrium and titanium, indicating Y–Ti complex nano-oxides. Particles in K4 contained yttrium and aluminum, indicating Y–Al complex nano-oxides. The figure also shows that the K4 steel contains coarse titanium-rich precipitates with segregation of tungsten in their surface.

As shown in Fig. 4, both alloys contain stringer-like precipitates, which align on the grain boundaries in the longitudinal direction. Most of the stringer-like precipitates identified as $M_{23}C_6$ type carbides by electron diffraction and EDS results, where M is Fe for 46 wt%, Cr for 48 wt% and W for 5 wt%.

XRD results of extracted residues of the K1 and K4 are displayed in Fig. 5. Both steels exhibit a considerable volume fraction of $M_{23}C_6$ carbides. In addition to this, only cubic pyrochlore type $Y_2Ti_2O_7$ oxide [9] is found in K1 steel, but none in K4. The XRD peaks from K4 exhibit mainly TiC (initially thought to be carbo-nitride) and perovskite $AlYO_3$ (YAP) peaks [10]. Very weak peaks from Al_2O_3 are found in K4.

3.2. Tensile test results and post-deformation microstructures

Yield stress data obtained from tensile tests at temperatures from room temperature to 900 °C for K1 and K4 steels are shown in Fig. 6. The data for MA956 (Fe–20Cr–4.5Al–0.34Ti–0.5Y_2O_3), MA957 (Fe–14Cr–1Ti–0.25Y_2O_3), PM2000 (Fe–20Cr–5.5Al–0.5Ti–0.5Y_2O_3), 12Y1 (Fe–12Cr–0.25Y_2O_3) and 12YWT (Fe–12Cr–2.5W–0.4Ti–0.25Y_2O_3) obtained and summarized by Klueh et al. [11] are also shown in the figure. The yield stress of the K1 steel is larger than that of the K4

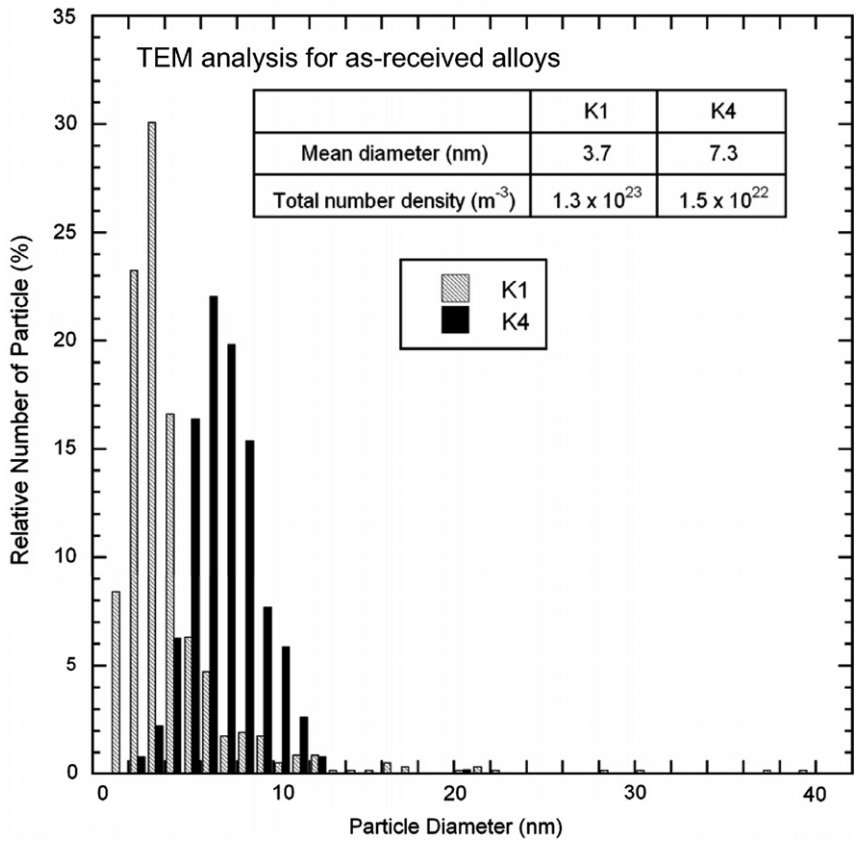

Fig. 2. Size distributions of oxide particles in the K1 and K4 steels evaluated from TEM micrographs.

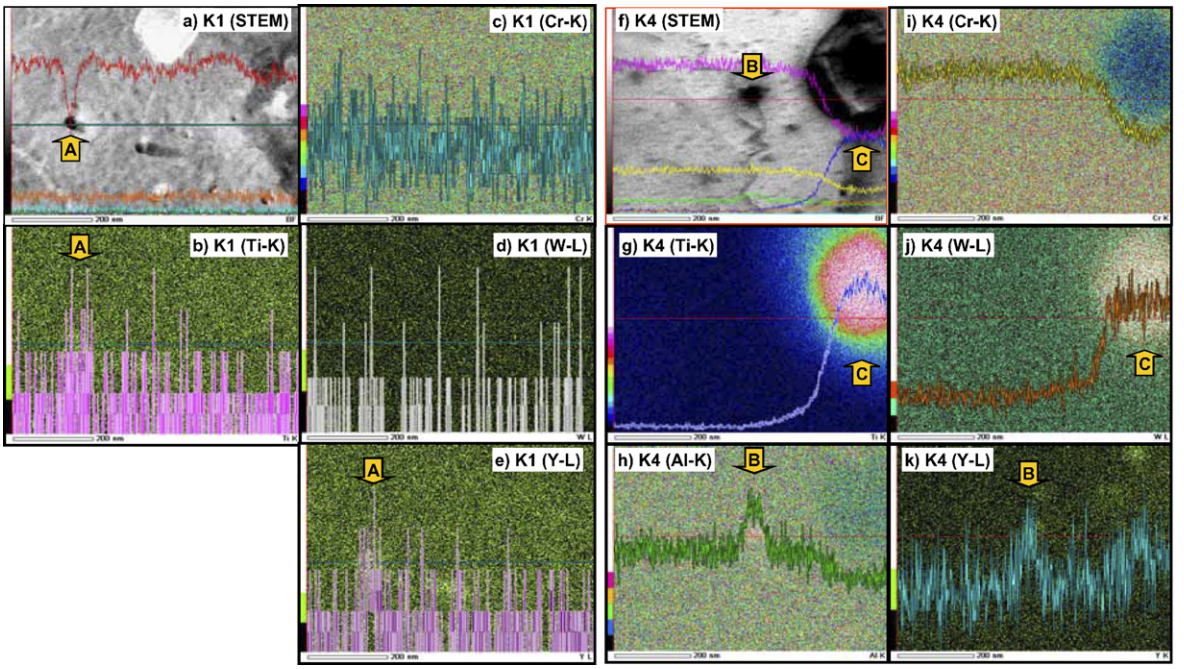

Fig. 3. Chemical profiles around oxide particles in K1 (a–e) and K4 (f–k) by using STEM-EDS: (a,f) STEM images; (b–e) and (g–k) present a series of EDS element mapping and line analyses revealing Cr, Ti, W, Y and Al.

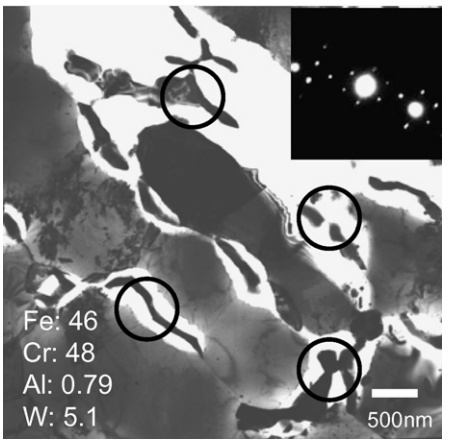

Fig. 4. TEM micrograph of $M_{23}C_6$ in the ODS steel with examples circled.

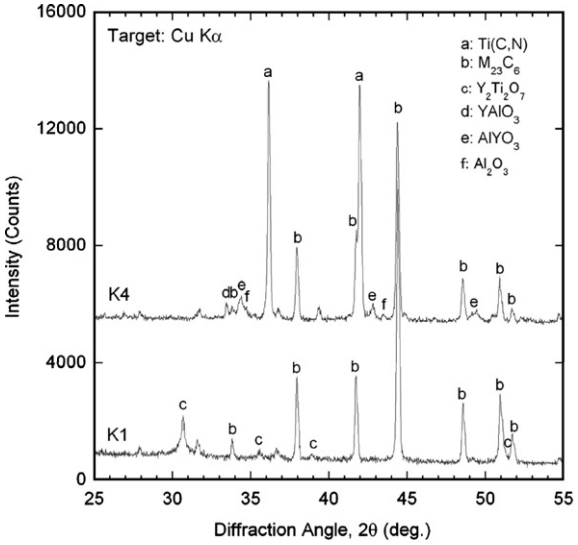

Fig. 5. XRD results of extracted residues from K1 and K4 steels.

ODS steel. Compared to the other ODS steels, K1 has similar strength to MA957 and 12YWT, and K4 has similar strength to PM2000 and 12Y1 for temperatures lower than 600 °C and to MA956 above 600 °C.

Fig. 7 shows TEM micrographs of the deformed area in the (a) K1 after tensile test at 400 °C and K4 after tensile tests at (b) 400 °C, (c) 600 °C and (d) 800 °C. The specimens were prepared from the area of 5–7 mm away from the fracture surface of the deformed tensile specimens. K1 and K4 tested at 400 °C show a high density of dislocations, which are tangled with nano-oxide particles. Conversely, specimens tested at 600 °C and 800 °C show a low density of dislocations with some pinning at oxide particles.

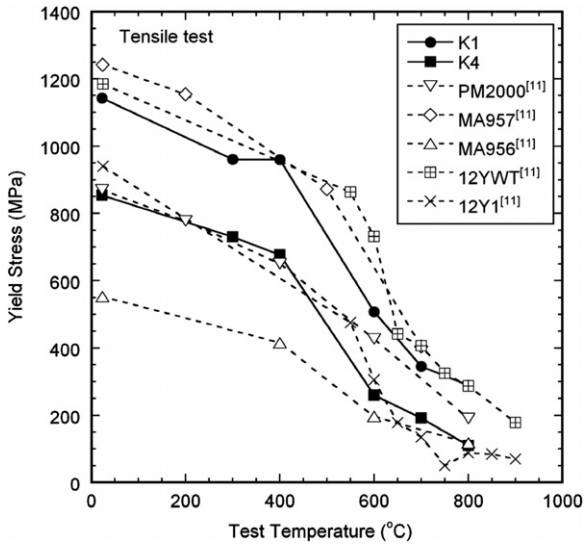

Fig. 6. Temperature dependence of 0.2% proof stress evaluated from tensile tests for the K1 and K4 steels with other ODS F/M steels.

4. Discussion

As shown in Fig. 2, size distribution and number density of the nano-oxide particles in K1 are substantially different from those in K4. The difference should be due to the compositional differences between the nano-oxides. As shown in Fig. 3, the STEM-EDS analyses indicated that mechanically-alloyed Y_2O_3 reacted with dissolved titanium in K1 steel and aluminum in K4 steel. This agrees very well with the XRD results on the extracted residues, showing $Y_2Ti_2O_7$ for K1 and YAP for K4, as shown in Fig. 5. The $Y_2Ti_2O_7$ complex oxides were also observed in the experimental 9Cr-ODS using a high resolution TEM by Yamashita et al. [12] and Klimiankou et al. [13]. As for the Y–Al complex oxides, previous studies showed a variety of results as follows: Dubiel et al. confirmed that the most of Y–Al oxides in MA956 is tetragonal $Y_3Al_5O_{12}$ (YAT) [14]. Czyrska-Filemonowicz et al. identified

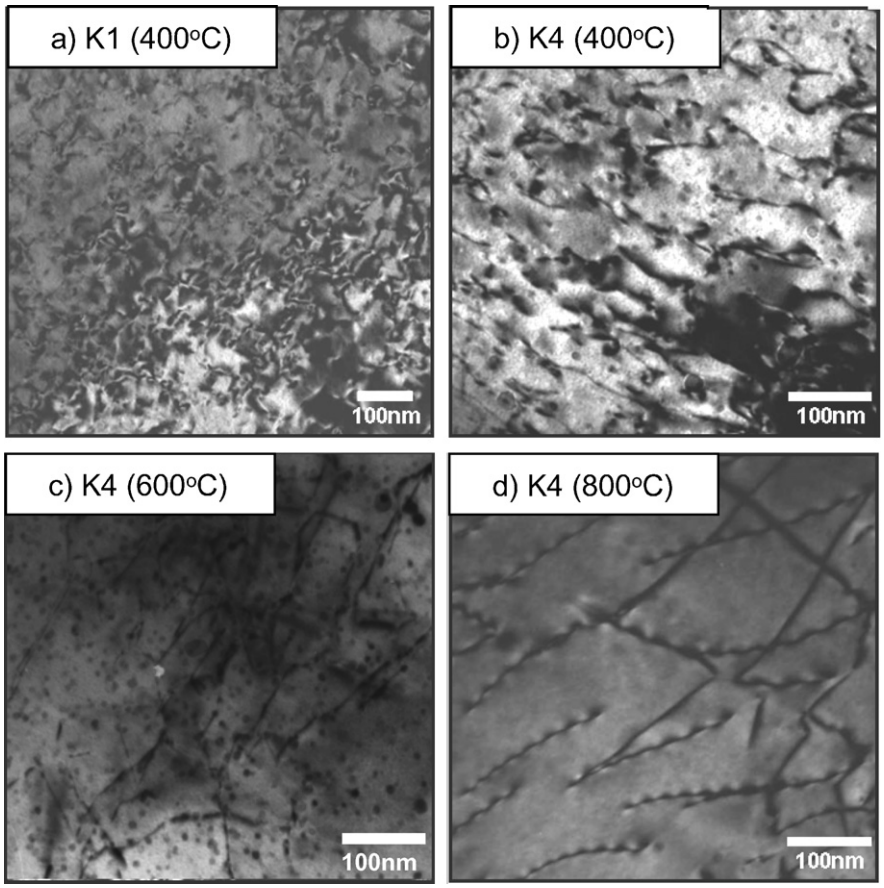

Fig. 7. TEM micrographs of the deformed areas in (a) K1 after a tensile test at 400 °C and in K4 after tensile tests at (b) 400 °C, (c) 600 °C and (d) 800 °C.

the Y–Al oxides in PM2000 as monoclinic $Y_4Al_2O_9$ (YAM) and YAT [15]. Krautwasser et al. showed that the isolated particles in PM2010 (Fe–20Cr–5.5Al–0.5Ti–1.0Y_2O_3) were garnet $Y_3Al_5O_{12}$ (YAG) and YAP [16]. These microstructural examinations lead to the conclusion that Y–Ti complex oxides were not present, but instead Y–Al complex oxides were formed when ODS F/M steels contain both aluminum and titanium. While the differences in the processing of ODS ferritic steels containing aluminum can cause the above-mentioned structural and compositional changes in the Y–Al complex oxides, further investigation is necessary.

The difference in the nano-oxides of K1 and K4 was reflected in differences in tensile properties, so that K1 has much higher strength than K4. Our previous report showed that the difference in the Orowan stress related to the nano-oxides of the K1 and K4 corresponded to differences in tensile yield stress at room temperature [8]. The experimental fact that the differences in yield stress are retained even at elevated temperatures, as shown in Fig. 6, can also support the explanation, since nano-oxide particles in the ODS steels should be very stable up to elevated temperature [16]. However, the difference in the yield stress decreases with increase in test temperatures above 600 °C because at high-temperatures thermal-activation processes control moving dislocations as shown in Fig. 7.

As-mentioned above, MA957 and 12YWT have similar strengths to K1, and PM2000 had similar strength to K4 below 600 °C. One possible explanation for these tendencies is that the former ODS F/M steels without aluminum addition have Y–Ti nano-oxides, typically $Y_2Ti_2O_7$, and the latter ones with aluminum addition have Y–Al nano-oxides. The difference in yield stress at room temperature and below 600 °C between K4 and MA956 is thought to be due to the difference in the heat treatment, as K4 steel is unrecrystallized while MA956 is completely recrystallized [11].

Most of the extracted residue in K1 and K4 was identified by XRD as $M_{23}C_6$ carbides. Moreover, TEM observations with EDS analysis revealed that inhomogeneous stringer-like $M_{23}C_6$ carbides align on the grain boundaries in the longitudinal direction for both the steels. These elongated and coarsened $M_{23}C_6$ carbides would probably cause anisotropic deformation and fracture behavior of the ODS ferritic steels [8]. Suppression of carbon contamination and optimization of heat treatments are expected to avoid $M_{23}C_6$ formation.

5. Conclusion

Pre- and post-deformation microstructures and tensile properties of the newly-developed ODS ferritic steels were investigated and conclusions are as follows:

(1) The nano-oxide morphology is different in K1 and K4 steels; the former contains $Y_2Ti_2O_7$ and the latter contains $AlYO_3$ (YAP), as confirmed by TEM, EDS and XRD analyses.
(2) The difference in the nano-oxides of K1 and K4 can account for the tensile test results showing K1 has much higher strength than K4.
(3) Most of the extracted residue in K1 and K4 was identified by XRD as $M_{23}C_6$ carbides.

Acknowledgements

The authors thank Professor H.K. Yoon and Dr D.H. Kim for performing tensile tests at elevated temperatures in Dong-Eui Univeristy.

References

[1] S. Ukai, T. Narita, A. Alamo, P. Parmentier, J. Nucl. Mater. 329–333 (2004) 356.
[2] M.B. Toloczko, D.S. Gelles, F.A. Garner, R.J. Kurtz, K. Abe, J. Nucl. Mater. 329–333 (2004) 352.
[3] A. Kimura, H.S. Cho, N. Toda, R. Kasada, H. Kishimoto, N. Iwata, S. Ukai, M. Fujiwara, in: Proceedings of the 2005 International Congress on Advances in Nuclear Power Plants (ICAPP '05), Seoul, Korea, 2005, p. 5338.
[4] N.Y. Iwata, A. Kimura, S. Ukai, M. Fujiwara, N. Kawashima, in: Proceedings of the 2005 International Congress on Advances in Nuclear Power Plants (ICAPP '05), Seoul, Korea, 2005, p. 5528.
[5] H.S. Cho, A. Kimura, S. Ukai, M. Fujiwara, J. Nucl. Mater. 329–333 (2004) 387.
[6] J.S. Lee, A. Kimura, S. Ukai, M. Fujiwara, J. Nucl. Mater. 329–333 (2004) 1122.
[7] H.S. Cho, H. Ohkubo, N.Y. Iwata, A. Kimura, S. Ukai, M. Fujiwara, in: Proceedings of the 2005 International Congress on Advances in Nuclear Power Plants (ICAPP '05), Seoul, Korea, 2005, p. 5457.
[8] R. Kasada, N. Toda, H.S. Cho, A. Kimura, in: Proceedings of the 2005 International Congress on Advances in Nuclear Power Plants (ICAPP '05), Seoul, Korea, 2005, p. 5328.
[9] N. Mizutani, A. Kitazawa, M. Kato, Nippon Kagaku Kaishi (9) (1974) 1623.
[10] T. Noguchi, M. Mizuno, Kogyo Kagaku Zasshi 70 (1967) 36.
[11] R.L. Klueh, J.P. Shingledecker, R.W. Swindeman, D.T. Hoelzer, J. Nucl. Mater. 341 (2005) 103.

[12] S. Yamashita, N. Akasaka, S. Ohnuki, J. Nucl. Mater. 329–333 (2004) 377.
[13] M. Klimiankou, R. Lindau, A. Möslang, J. Nucl. Mater. 329–333 (2004) 347.
[14] B. Dubiel, W. Osuch, M. Wróbel, P.J. Ennis, A. Czyrsk-Filemonowicz, J. Mater. Process. Technol. 53 (1995) 121.
[15] A. Czyrska-Filemonowicz, D. Clemens, W.J. Quadakkers, J. Mater. Process. Technol. 53 (1995) 93.
[16] P. Krautwasser, A. Czyrska-Filemonowicz, M. Widera, F. Carsughi, Mater. Sci. Eng. A 177 (1994) 199.